Testing global isotropy of three-year Wilkinson Microwave Anisotropy Probe (WMAP) data: Temperature analysis

Amir Hajian

Department of Physics, Jadwin Hall, Princeton University, PO Box 708, Princeton, New Jersey 08542, USA
and Department of Astrophysical Sciences, Peyton Hall, Princeton University, Princeton, New Jersey 08544, USA

Tarun Souradeep

Inter-University Centre for Astronomy and Astrophysics (IUCAA), Ganeshkhind, Pune-411007, India
(Received 25 July 2006; revised manuscript received 11 October 2006; published 29 December 2006)

We examine statistical isotropy of large scale anisotropies of the Internal Linear Combination (ILC) map, based on 3 yr WMAP data. Our study reveals no significant deviation from statistical isotropy on large angular scales of the 3 yr ILC map. Comparing statistical isotropy of the 3 yr ILC map and 1 yr ILC map, we find a significant improvement in the 3 yr ILC map which can be due to the gain model, improved ILC map processing, and foreground minimization.

DOI: 10.1103/PhysRevD.74.123521 PACS numbers: 98.70.Vc, 98.80.Es

I. INTRODUCTION

The cosmic microwave background (CMB) anisotropy has been shown to be a very powerful observational probe of cosmology. Detailed measurements of the anisotropies in the CMB can provide a wealth of information about the global properties, constituents, and history of the Universe. In standard cosmology, the CMB anisotropy is expected to be statistically isotropic, i.e., statistical expectation values of the temperature fluctuations (and, in particular, the angular correlation function) are preserved under rotations of the sky. This property of CMB anisotropy has been under scrutiny after the release of the first year of WMAP data [1–25]. We use a method based on bipolar expansion of the two-point correlation function which is an improved and enhanced follow-up on our previous work on first year WMAP data [25,26]. This method is shown to be sensitive to structures and patterns in the underlying two-point correlation function.

We apply our method to the improved Internal Linear Combination (ILC) map [27], based on 3 yr WMAP data [28]. We choose the ILC map for testing statistical isotropy (SI) of the CMB anisotropy for the following reasons:

(1) The ILC is a full-sky map and hence is easier to work with. Masking the sky results in violation of statistical isotropy. An originally SI CMB anisotropy map deviates from SI after masking [26].
(2) Residuals from galactic removal errors in the 3 yr ILC map are estimated to be less than 5 μK on angular scales greater than $\sim$10 deg [27]. Hence at low-l, multipoles are not significantly affected by foregrounds. In addition, it is interesting to examine the above statement by testing the statistical isotropy of the ILC map.
(3) On large scales, the 3 yr ILC map is believed to provide a reliable estimate of the CMB signal, with negligible instrument noise, over the full sky [27]. These properties of the ILC map allow us to study the cosmological signal on large scales. In addition, there are theoretical motivations for hunting for SI violation on large scales of CMB anisotropy. Topologically compact spaces [29–32] and anisotropic cosmological models [33–39] are examples of this. Both observational artifacts and the above theoretical models cause a departure from statistical isotropy and it has been shown that our method is a useful tool to find out these deviations (see e.g. [39–42]). The rest of this paper is organized as follows: Section II is a brief introduction to temperature anisotropy of CMB. Section III describes the formulation of statistical isotropy in general. Section IV is a description of estimators we use to look for deviations from statistical isotropy. We present the application of our method on the WMAP data in Sec. V. Section VI contains discussion on the cosmological implications of our null detection of deviations from statistical isotropy on large angular scales in the 3 yr ILC map of WMAP data, and in Sec. VII we summarize our results.

II. CHARACTERIZATION OF CMB TEMPERATURE ANISOTROPY

The CMB anisotropy is fully described by its temperature anisotropy and polarization. The temperature anisotropy is a scalar random field, $\Delta T(\hat{n}) = T(\hat{n}) - T_0$, on a 2-dimensional surface of a sphere (the sky), where $\hat{n} = (\theta, \phi)$ is a unit vector on the sphere and $T_0 = \int \frac{d\Omega_{\hat{n}}}{4\pi} T(\hat{n})$ represents the mean temperature of the CMB. It is convenient to expand the temperature anisotropy field into spherical harmonics, the orthonormal basis on the sphere, as

$$\Delta T(\hat{n}) = \sum_{l,m} a_{lm} Y_{lm}(\hat{n}), \tag{1}$$

where the complex quantities a_{lm} are given by

$$a_{lm} = \int \mathrm{d}\Omega_{\hat{n}} Y^*_{lm}(\hat{n}) \Delta T(\hat{n}). \quad (2)$$

Statistical properties of this field can be characterized by n-point correlation functions

$$\langle \Delta T(\hat{n}_1) \Delta T(\hat{n}_2) \cdots \Delta T(\hat{n}_n) \rangle. \quad (3)$$

Here the bracket denotes the ensemble average, i.e. an average over all possible configurations of the field. CMB anisotropy is believed to be Gaussian [43,44]. Hence the connected part of n-point functions disappears for $n > 2$. Nonzero (even-n)-point correlation functions can be expressed in terms of the two-point correlation function. As a result, a Gaussian distribution is completely described by the two-point correlation function

$$C(\hat{n}, \hat{n}') = \langle \Delta T(\hat{n}) \Delta T(\hat{n}') \rangle. \quad (4)$$

Equivalently, as it is seen from Eq. (2), for a Gaussian CMB anisotropy, a_{lm} are complex Gaussian random variables too. Therefore, the *covariance matrix* $\langle a_{lm} a^*_{l'm'} \rangle$ fully describes the whole field. Throughout this paper we assume Gaussianity to be valid.

III. STATISTICAL ISOTROPY

Two-point correlations of CMB anisotropy, $C(\hat{n}_1, \hat{n}_2)$, are two-point functions on $S^2 \times S^2$, and hence can be expanded as

$$C(\hat{n}_1, \hat{n}_2) = \sum_{l_1, l_2, \ell, M} A_{\ell M | l_1 l_2} Y^{l_1 l_2}_{\ell M}(\hat{n}_1, \hat{n}_2). \quad (5)$$

Here $A_{\ell M | l_1 l_2}$ are coefficients of the expansion (hereafter BipoSH coefficients) and $Y^{l_1 l_2}_{\ell M}(\hat{n}_1, \hat{n}_2)$ are bipolar spherical harmonics defined by Eq. (A1). Bipolar spherical harmonics form an orthonormal basis on $S^2 \times S^2$ and transform in the same manner as the spherical harmonic function with ℓ, M with respect to rotations [45]. One can inverse transform $C(\hat{n}_1, \hat{n}_2)$ in Eq. (5) to get the coefficients of expansion, $A_{\ell M | l_1 l_2}$, by multiplying both sides of Eq. (5) by $Y^{*l_1' l_2'}_{\ell' M'}(\hat{n}_1, \hat{n}_2)$ and integrating over all angles. Then the orthonormality of bipolar harmonics, Eq. (A3), implies that

$$A_{\ell M | l_1 l_2} = \int d\Omega_{\hat{n}_1} \int d\Omega_{\hat{n}_2} C(\hat{n}_1, \hat{n}_2) Y^{*l_1 l_2}_{\ell M}(\hat{n}_1, \hat{n}_2). \quad (6)$$

The above expression and the fact that $C(\hat{n}_1, \hat{n}_2)$ is symmetric under the exchange of $\hat{n}_1$ and $\hat{n}_2$ leads to the following symmetries of $A_{\ell M | l_1 l_2}$

$$A_{\ell M | l_2 l_1} = (-1)^{(l_1 + l_2 - \ell)} A_{\ell M | l_1 l_2}, \qquad A_{\ell M | l l} = A_{\ell M | l l} \delta_{\ell, 2k}, \quad k = 0, 1, 2, 3, \cdots. \quad (7)$$

It has been shown [26] that bipolar spherical harmonic (BipoSH) coefficients, $A_{\ell M | l_1 l_2}$, are in fact linear combinations of off-diagonal elements of the covariance matrix

$$A_{\ell M | l_1 l_2} = \sum_{m_1 m_2} \langle a_{l_1 m_1} a^*_{l_2 m_2} \rangle (-1)^{m_2} \mathcal{C}^{\ell M}_{l_1 m_1 l_2 - m_2}, \quad (8)$$

where $\mathcal{C}^{\ell M}_{l_1 m_1 l_2 m_2}$ are Clebsch-Gordan coefficients (see the appendix). This clearly shows that $A_{\ell M | l_1 l_2}$ completely represent the information of the covariance matrix. When statistical isotropy holds, it is guaranteed that the covariance matrix is diagonal,

$$\langle a_{lm} a^*_{l'm'} \rangle = C_l \delta_{ll'} \delta_{mm'} \quad (9)$$

and hence the angular power spectra carry all information of the field. Substituting this into Eq. (8) gives

$$A_{\ell M | l l'} = (-1)^l C_l (2l + 1)^{1/2} \delta_{ll'} \delta_{\ell 0} \delta_{M 0}. \quad (10)$$

The above expression tells us that when statistical isotropy holds, all BipoSH coefficients, $A_{\ell M | l l'}$, are zero except those with $\ell = 0$, $M = 0$ which are equal to the angular power spectra up to a $(-1)^l (2l + 1)^{1/2}$ factor. BipoSH expansion is the most general way of studying two-point correlation functions of CMB anisotropy. The well-known angular power spectrum C_l is in fact a subset of the corresponding BipoSH coefficients,

$$C_l = \frac{(-1)^l}{\sqrt{2l + 1}} A_{00 | l l}. \quad (11)$$

Therefore to test a CMB map for statistical isotropy, one should compute the BipoSH coefficients for the maps and look for nonzero BipoSH coefficients. Statistically significant deviations from zero would mean violation of statistical isotropy.

IV. ESTIMATORS

Given a CMB anisotropy map, one can measure BipoSH coefficients by the following estimator [46]

$$\tilde{A}_{\ell M | l l'} = \sum_{m m'} \sqrt{W_l W_{l'}}\, \tilde{a}_{lm} \tilde{a}_{l' m'} \mathcal{C}^{\ell M}_{l m l' m'}, \quad (12)$$

where W_l is the Legendre transform of the window function. The above estimator is a combination of C_l and hence is unbiased [47]. However it is impossible to measure all $A_{\ell M | l l'}$ individually because of cosmic variance. Combining BipoSH coefficients helps to reduce the cosmic variance [48]. There are several ways of combining BipoSH coefficients. Here we choose two methods.

A. First method: BiPS

Among the several possible combinations of BipoSH coefficients, the bipolar power spectrum (BiPS) was proved to be a useful tool with interesting features [49]. BiPS of CMB anisotropy is defined as a convenient contraction of the BipoSH coefficients

$$\kappa_\ell = \sum_{l, l', M} |A_{\ell M | l l'}|^2 \geq 0. \quad (13)$$

BiPS is interesting because it is orientation independent, i.e. invariant under rotations of the sky. For models in which statistical isotropy is valid, BipoSH coefficients are given by Eq. (10), and therefore SI condition implies a null BiPS, i.e. $\kappa_\ell = 0$ for every $\ell > 0$,

$$\kappa_\ell = \kappa_0 \delta_{\ell 0}. \tag{14}$$

Nonzero components of BiPS imply breakdown of statistical isotropy, and this introduces BiPS as a measure of statistical isotropy. It is worth noting that although BiPS is quartic in a_{lm}, it is designed to detect SI violation and not non-Gaussianity [25,26,49–51]. An unbiased estimator of BiPS is given by

$$\tilde{\kappa}_\ell = \sum_{ll'M} |\tilde{A}_{\ell M|ll'}|^2 - \mathfrak{B}_\ell, \tag{15}$$

where $\mathfrak{B}_\ell$ is the bias that arises from the SI part of the map and is given by the angular power spectrum C_l,

$$\begin{aligned}\mathfrak{B}_\ell &\equiv \langle \tilde{\kappa}^B_\ell \rangle_{\rm SI} \\ &= (2\ell+1)\sum_{l_1} \sum_{l_2=|\ell-l_1|}^{\ell+l_1} W_{l_1} W_{l_2} [C_{l_1} C_{l_2} \\ &\quad + (-1)^\ell \delta_{l_1 l_2} (C_{l_1})^2]. \end{aligned} \tag{16}$$

The above expression for $\mathfrak{B}_\ell$ is obtained by assuming Gaussian statistics of the temperature fluctuations [26,49].

B. New method: reduced bipolar coefficients

The BipoSH coefficients of Eq. (12) can be summed over l and l' to reduce the cosmic variance

$$A_{\ell M} = \sum_{l=0}^{\infty} \sum_{l'=|\ell-l|}^{\ell+l} A_{\ell M|ll'}. \tag{17}$$

These reduced bipolar coefficients, $A_{\ell M}$, by definition respect the following symmetry:

$$A_{\ell M} = (-1)^M A^*_{\ell -M}, \tag{18}$$

which indicates $A_{\ell 0}$ are always real. When SI condition is valid, the ensemble average of $A_{\ell M}$ vanishes for all ℓ and M

$$\langle A_{\ell M} \rangle = 0. \tag{19}$$

In any given CMB anisotropy map, $A_{\ell M}$ would fluctuate about zero. A severe breakdown of statistical isotropy will result in huge deviations from zero. Reduced bipolar coefficients are not rotationally invariant, hence they assign direction to the correlation patterns of a map. We can combine $A_{\ell M}$ further to define a power spectrum similar to how a_{lm} are combined to construct the angular power spectrum, C_l. We define

$$D_\ell = \frac{1}{2\ell+1} \sum_{M=-\ell}^{\ell} A_{\ell M} A^*_{\ell M}. \tag{20}$$

The above estimator is rotationally invariant. It has a positive bias and hence it has similar issues that have been addressed for the BiPS studies earlier. This means although the ensemble average of $A_{\ell M}$ for a statistically isotropic case is zero, the ensemble average of D_ℓ is always greater than zero. However a major deviation from statistical isotropy will result in a big D_ℓ (compared to that of a SI case). In Sec. V we compare $A_{\ell M}$ of the ILC map against an average of 1000 simulations of statistically isotropic maps. We defer detailed studies of D_ℓ to the future publication.

V. APPLICATION TO THE WMAP DATA

We carry out our analysis on the 3 yr ILC map and compare it to 1 yr ILC map [52]. In order to attribute a statistical significance to our results, we compare our results to 1000 simulations of SI CMB maps. a_{lm}'s of these maps are generated up to an $l_{\rm max}$ of 1024 (corresponding to HEALPix [53] resolution $N_{\rm side} = 512$). Since we are only interested in large angular scales we smooth all maps with appropriate filters to cut the power on small angular scales. These filters are low-pass Gaussian filters

$$W^G_l = N^G \exp\left\{-\left(\frac{2l+1}{2l_s+1}\right)^2\right\} \tag{21}$$

that cut power on scales ($l \geq l_s$) and band pass filters of the form

$$W^S_l = 2N^S\left[1 - J_0\left(\frac{2l+1}{2l_t+1}\right)\right]\exp\left\{-\left(\frac{2l+1}{2l_s+1}\right)^2\right\}, \tag{22}$$

that keep the power on scales corresponding to $l_t < l < l_s$. J_0 is the bessel function and N^G and N^S are normalization constants chosen such that

$$\sum_l \frac{(2l+1)W_l}{2l(l+1)} = 1, \tag{23}$$

i.e., unit rms for unit flat band angular power spectrum $C_l = \frac{2\pi}{l(l+1)}$.

We compute the BipoSH coefficients, $A_{\ell M|ll'}$, for the 3 yr ILC map (ILC-3) for several window functions using Eq. (12). We combine these coefficients using Eq. (17) to obtain $A_{\ell M}$. An interesting way of visualizing these coefficients is to make a map from them. Making a map from $A_{\ell M}$ is simply done similar to making a temperature anisotropy map from a given set of spherical harmonic coefficients, a_{lm};

$$\Theta(\hat{n}) = \sum_{\ell=0}^{\infty} \sum_{M=-\ell}^{\ell} A_{\ell M} Y_{\ell M}(\hat{n}). \tag{24}$$

The symmetry of reduced bipolar coefficients, Eq. (18), guarantees reality of $\Theta(\hat{n})$. The "bipolar" map based on bipolar coefficients of ILC-3 is shown in the top panel of Fig. 1. The map has small fluctuations except for a pair of hot and cold spots near the equator. To compare, we have

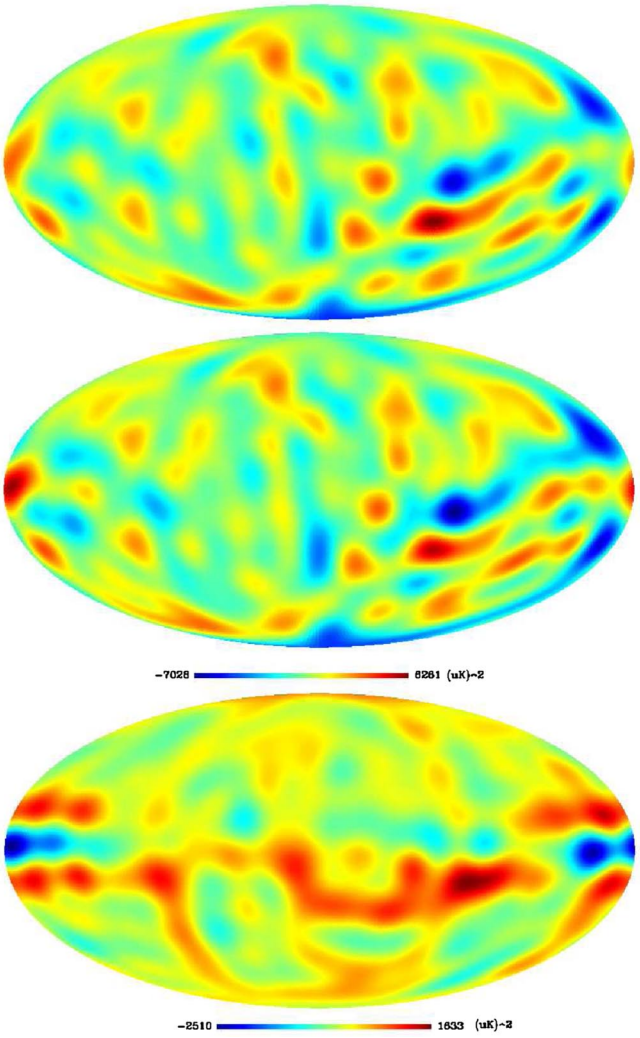

FIG. 1 (color online). Top: A *bipolar* map generated from bipolar coefficients $A_{\ell M}$ of the 3 yr ILC map. Middle: bipolar map based on the 1 yr ILC map. Bottom: differences between the two maps (note the scales). The top map (ILC-3) has smaller fluctuations comparing to the middle one (ILC-1) except for the hot spot near the equator. Differences between these two maps mostly arise from a band around the equator *in bipolar space*. Both ILC maps are smoothed by a band pass filter, $W^S(l_t = 2, l_s = 10)$.

also made a bipolar map of the 1 yr ILC map (ILC-1) from bipolar coefficients of ILC-1 (middle panel of Fig. 1). The difference map (Fig. 1 (bottom)) shows that differences between these two maps mostly arise from a band around the equator *in bipolar space*. As it is seen in Fig. 1, the bipolar map of ILC-3 has less fluctuations compared to that of ILC-1. This is because almost all of $A_{\ell M}$'s of ILC-3 are smaller than those of ILC-1 (i.e. are closer to zero). Reduced bipolar coefficients of the above maps are in Fig. 2, in which ℓ and M indices are combined to a single index $n = \ell(\ell + 1) + M + 1$ (only the real part of $A_{\ell M}$ is plotted). And the dotted lines define 1-σ error bars derived from 1000 simulations of SI CMB anisotropy maps. As can

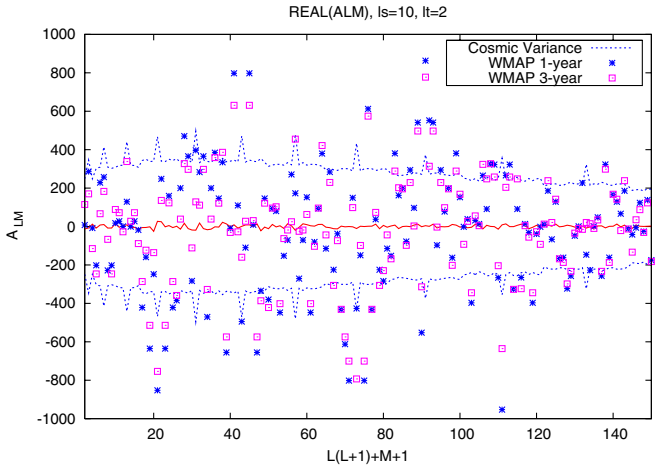

FIG. 2 (color online). Real part of $A_{\ell M}$'s of ILC-3 (square points) and ILC-1 (stars) for a $W^S(10, 2)$ filter that roughly keeps multipoles between 2 and 15. ℓ and M indices are combined to a single index $n = \ell(\ell + 1) + M + 1$ and the dotted lines define 1-σ error bars derived from 1000 simulations of SI CMB anisotropy maps. Almost all of the $A_{\ell M}$'s of ILC-3 are smaller than those of ILC-1 which means ILC-3 is more consistent with statistical isotropy.

be seen, many spikes in $A_{\ell M}$'s of ILC-1 have either disappeared or reduced in ILC-3 (e.g. those around $n = 20$, 40 and a big spike at $n = 111$). To get a quantitative description of differences between ILC-3 and ILC-1 we compare them against 1000 simulations of SI CMB anisotropy maps. A simple χ^2 comparison of $A_{\ell M}$ with simulations gives us a rough estimate of overall differences between the two ILC maps: ILC-3 has a smaller χ^2 than ILC-1. For a $W^S(10, 2)$ filter, the reduced χ^2 falls from 1.089 for ILC-1 to 0.9619 for ILC-3. Although the χ^2 statistic is simple, it should be used with caution because it is only valid if every $A_{\ell M}$ is independent and has a Gaussian distribution function. In order to study deviations of $A_{\ell M}$ from zero without worrying about the Gaussianity of the $A_{\ell M}$, we look at the most deviant (biggest) $A_{\ell M}$. We compare the biggest $A_{\ell M}$'s of ILC to $A_{\ell M}$'s of 1000 simulations to find out what fraction of simulations have $A_{\ell M}$'s smaller than those of ILC maps. Figure 3 shows the results. The horizontal axis is $n = \ell(\ell + 1) + M + 1$ and the vertical axis is the fraction of $A_{\ell M}$'s in 1000 simulations that are smaller than $A_{\ell M}$ of ILC. In this figure, squares represent the ILC-1 while ILC-3 is represented by lines. When a line crosses a point, $A_{\ell M}$'s of ILC-3 are greater than ILC-1, otherwise points above the spikes show smaller $A_{\ell M}$'s for ILC-3. The results are interesting: several deviations in ILC-1 have been corrected in ILC-3. Especially on the largest scales, several deviations beyond 95% in ILC-1 have gone away in ILC-3 (the points above the dotted line in Fig. 3 have been replaced by significantly smaller values).

Combining the BipoSH coefficients to construct bipolar power spectrum allows further examinations of ILC maps

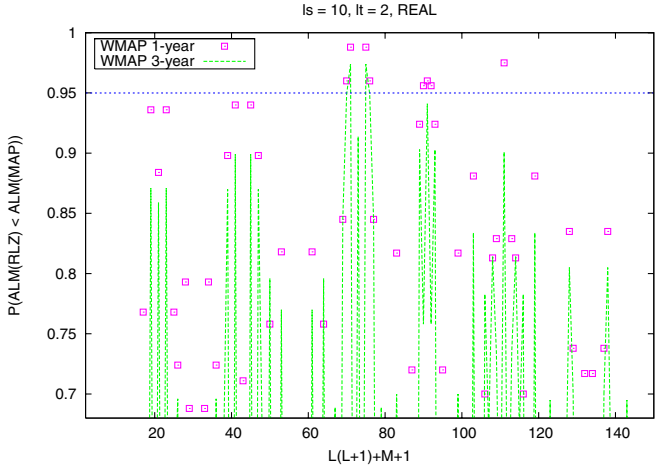

FIG. 3 (color online). Fraction of the $A_{\ell M}$'s in 1000 simulations that are smaller than the $A_{\ell M}$'s of ILC. Several deviations in ILC-1 (square points) have been corrected in ILC-3 (impulses). Only deviations above 68% are shown. Almost all of the $A_{\ell M}$'s of ILC-3 are smaller than those of ILC-1 which means ILC-3 is more consistent with statistical isotropy. Only real parts are shown. Points are always in pairs because of the symmetry in reduced bipolar coefficients, $A_{\ell M} = (-1)^M A^*_{\ell -M}$. All maps are smoothed with a $W^S(10, 2)$ filter.

for departures from SI. We compute the BiPS using Eq. (15). It is worth mentioning that BiPS in this paper has been computed in a slightly different way than in our previous paper [25]. Here we compute the BiPS using Eq. (15) and we use the derived C_l from each map to estimate the bias $\mathfrak{B}_\ell$ using Eq. (16) [54]. The bias corrected BiPS is then averaged over 1000 simulations and is compared to the bias corrected BiPS of ILC maps. BiPS results

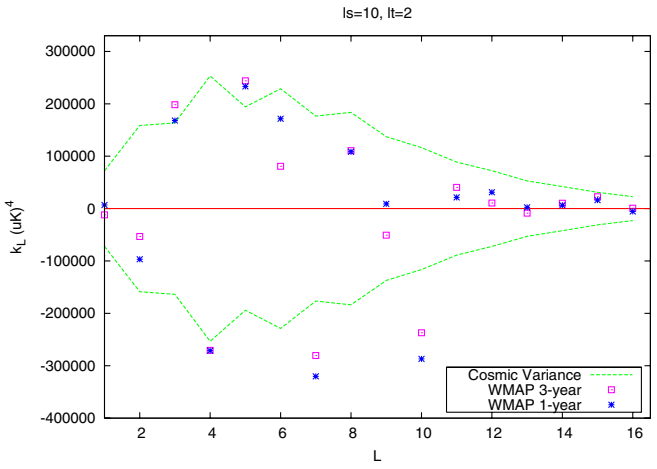

FIG. 4 (color online). Bipolar power spectrum of the two ILC maps compared to the average BiPS of 1000 simulations of statistically isotropic CMB maps. Both ILC maps are smoothed with a $W^S(10, 2)$ window function which roughly retains multipoles in the range of $2 \leq l \leq 15$. ILC-3 shows smaller BiPS than ILC-1, which means it is more consistent with statistical isotropy. Filtering the data with other functions show almost the same results.

shown in Fig. 4 agree with our results on $A_{\ell M}$. It can be seen that ILC-3 has a smaller bipolar power spectrum than ILC-1 and is more consistent with statistical isotropy. The same is true for the D_ℓ estimator defined by Eq. (20) which we defer to the future publications. We should emphasize that these results are only for large angular scales, $l \leq 25$, and not beyond that.

VI. DISCUSSION AND CONCLUSIONS

The null results of search for departure from statistical isotropy has implications for the observation and data analysis techniques used to create the CMB anisotropy maps. Observational artifacts such as the noncircular beam, inhomogeneous noise correlation, residual striping patterns, and residuals from foregrounds are potential sources of SI breakdown. Our null results confirm that these artifacts do not significantly contribute to large scale anisotropies of the 3 yr ILC map (see [26,41,42] for more details). We have also quantified the differences between the 1 yr and 3 yr ILC maps. It is shown that the 3 yr ILC map is "cleaner" than the 1 yr ILC map at $l \leq 25$. This can be due to the gain model and improved ILC map processing and foreground minimization. We limit ourselves to the low-l limit because in addition to observational artifacts, there are theoretical motivations for hunting for SI violation on large scales of CMB anisotropy. Topologically compact spaces [29–32] and anisotropic cosmological models [33–39] are examples of this. Each of these models will cause departures from statistical isotropy in CMB anisotropy maps. And a null detection of departure from statistical isotropy at low l in the WMAP data can be used to put constraints on these models. To prove that the null detection is meaningful, it should be shown that the method is actually capable of detecting potential anomalies in CMB anisotropy maps. Below we point out some examples of violation of statistical isotropy which our method has been shown to be able to detect. Most of them have been studied in previous publications.

(1) *Anisotropic cosmological models [Bianchi models]*: Bianchi VII$_h$ models have been proposed to explain potential anomalies in the CMB anisotropy as observed by WMAP [38]. These anisotropic patterns have a nonzero bipolar power spectrum. BiPS has been used to test the consistency of embedded Bianchi VII$_h$ templates in the CMB anisotropy maps with the WMAP data and a limit of $(\sigma/H)_0 > 2.55 \times 10^{-10}$ (99.9% C.L.) was put on the shear parameter in Bianchi VII$_h$ models by examining the statistical isotropy of these maps [39].

(2) *Compact spaces*: The CMB sky maps in spatially compact universe models violate statistical isotropy. This breakdown of statistical isotropy usually manifests itself as underlying correlation patterns on large angular separation (that would correspond to large physical separation in a universe with trivial

topology). The patterns reflect the existence of preferred directions in these models. Bipolar power spectrum signatures of statistical isotropy violation in compact spaces have been studied. It has been shown that BiPS can be numerically computed for these models from their two-point correlation matrices and the results can be understood (and predicted) using the leading order terms of the correlation function in a torus where BiPS can be calculated analytically. This has been studied in [40] and in more details in the Ph.D. thesis [41].

(3) *Foreground contamination*: Statistical isotropy violation due to foreground contamination was studied in a recent publication where a generalization of the BiPS to polarization maps has been presented [55]. As a demonstration it has been shown that for E-polarization this test can detect the breakdown of statistical isotropy due to polarized synchrotron foreground.

(4) *Residuals from foregrounds in temperature maps*: The signature of residuals from foregrounds in our measure has been studied and the result will be reported in a future publication. The foreground cleaned maps obtained as part of an independent CMB power spectrum estimation from WMAP-1 in [56] show traces of foreground residuals along the galactic plane. These provide ideal, ''real life'' case study material for the bipolar analysis. These maps show clear measurable violation of statistical isotropy in terms of a characteristic nonzero bipolar power spectrum. We find that BiPS can distinguish between the quality of maps made with different iteration levels of cleaning algorithm (where the actual differences are very small but have a pattern).

(5) *Anisotropic noise*: The CMB temperature measured by an instrument is a linear sum of the cosmological signal as well as instrumental noise. Both signal and noise should be statistically isotropic to have a statistically isotropic CMB map. So even for a statistically isotropic signal, if the noise fails to be statistically isotropic the resultant map will turn out to be anisotropic. This effect has been studied using BiPS [26,41].

(6) *Galactic cut*: The incomplete sky or mask effect is another source of breakdown of SI. This effect has been studied using BiPS in [26] in both analytical and numerical ways. Especially a galactic mask was applied to an originally SI CMB anisotropy map and it was shown that the signature of this mask on BiPS is a rising tail at bipolar ℓ, ($\ell < 20$).

Our measure is sensitive to axial asymmetries in the two-point correlation of the temperature anisotropy [40]. And this is even more significant now because the new measure of reduced bipolar coefficients does retain directional information. Our analysis does not show a significant detection of an ''axis of evil'' in the WMAP data. We have redone our analysis on the ILC map filtered with a low-pass filter that only keeps $l = 2, 3, 4$ to search for a preferred direction at low multipoles. We have not been able to detect any significant deviation from statistical isotropy using various filters. We could not test the reported specific alignments of low multipoles since those results were not posed in terms of an underlying model for the correlation [57]. Validity of statistical isotropy at large angular scales can put tight constraints on anisotropic mechanisms that are candidates of explaining the low quadrupole of WMAP and COBE data. It is worth noticing that our method can be extended to polarization maps of CMB anisotropy [55,58]. Analysis of statistical isotropy of full-sky polarization maps of WMAP are currently under progress and will be reported in a separate publication.

VII. SUMMARY

We examine statistical isotropy of large scale anisotropies of the improved the ILC map, based on 3 yr WMAP data. In order to attribute a statistical significance to our results, we use 1000 simulations of statistically isotropic CMB maps. We have done our analysis using a series of filters that span the low-l multipoles. We only explicitly present the results for one of them that roughly retains power in the multipoles between 2 and 15. This reveals no significant deviation from statistical isotropy on large angular scales of the 3 yr ILC map. Comparing statistical isotropy of the 3 yr ILC map and 1 yr ILC map, we find a significant improvement in the 3 yr ILC map which can be due to the gain model and improved ILC map processing and foreground minimization. We get consistent and similar results from other filters.

ACKNOWLEDGMENTS

A. H. wishes to thank Lyman Page and David Spergel for enlightening discussions throughout this project. A. H. also thanks Soumen Basak for his careful reading and comments on the manuscript and Joanna Dunkley and Mike Nolta for useful discussions. Some of the results in this paper have used the HEALPix package. We acknowledge the use of the Legacy Archive for Microwave Background Data Analysis (LAMBDA) [59]. Support for LAMBDA is provided by the NASA Office of Space Science. A. H. acknowledges support from NASA Grant No. LTSA03-0000-0090.

APPENDIX: USEFUL MATHEMATICAL RELATIONS

Bipolar spherical harmonics form an orthonormal basis of $S^2 \times S^2$ and are defined as

$$Y^{l_1 l_2}_{\ell M}(\hat{n}_1, \hat{n}_2) = \sum_{m_1 m_2} \mathcal{C}^{\ell M}_{l_1 m_1 l_2 m_2} Y_{l_1 m_1}(\hat{n}_1) Y_{l_2 m_2}(\hat{n}_2), \qquad \text{(A1)}$$

in which $\mathcal{C}^{\ell M}_{l_1 m_1 l_2 m_2}$ are Clebsch-Gordan coefficients. Clebsch-Gordan coefficients are nonzero only if the triangularity relation holds, $\{l_1 l_2 \ell\}$, and $M = m_1 + m_2$. Where the $3j$-symbol $\{abc\}$ is defined by

$$\{abc\} = \begin{cases} 1 & \text{if } a+b+c \text{ is integer and } |a-b| \le c \le (a+b), \\ 0 & \text{otherwise,} \end{cases} \tag{A2}$$

Orthonormality of bipolar spherical harmonics

$$\int d\Omega_{\hat{n}_1} d\Omega_{\hat{n}_2} Y^{l_1 l_2}_{\ell M}(\hat{n}_1, \hat{n}_2) Y^{*l_1' l_2'}_{\ell' M'}(\hat{n}_1, \hat{n}_2) = \delta_{l_1 l_1'} \delta_{l_2 l_2'} \delta_{\ell \ell'} \delta_{M M'}. \tag{A3}$$

Symmetry properties of Clebsch-Gordan coefficients

$$\begin{aligned} C^{c\gamma}_{a\alpha b\beta} &= (-1)^{a+b-c} C^{c\gamma}_{b\beta a\alpha}, \\ C^{c\gamma}_{a\alpha b\beta} &= (-1)^{a+b-c} C^{c-\gamma}_{a-\alpha b-\beta}. \end{aligned} \tag{A4}$$

Summation rules of Clebsch-Gordan coefficients

$$\begin{aligned} \sum_{\alpha\beta} C^{c\gamma}_{a\alpha b\beta} C^{c'\gamma'}_{a\alpha b\beta} &= \delta_{cc'} \delta_{\gamma\gamma'} \{abc\}\{abc'\}, \\ \sum_{a\gamma} C^{c\gamma}_{a\alpha b\beta} C^{c\gamma}_{a\alpha b'\beta'} &= \frac{2c+1}{2b+1} \delta_{bb'} \delta_{\beta\beta'} \{abc\}\{ab'c\}, \\ \sum_{c\gamma} C^{c\gamma}_{a\alpha b\beta} C^{c\gamma}_{a\alpha' b\beta'} &= \delta_{\alpha\alpha'} \delta_{\beta\beta'} \{abc\}. \end{aligned} \tag{A5}$$

[1] H. K. Eriksen, F. K. Hansen, A. J. Banday, K. M. Gorski, and P. B. Lilje, Astrophys. J. **605**, 14 (2004); **609**, 1198(E) (2004).
[2] C. J. Copi, D. Huterer, and G. D. Starkman, Phys. Rev. D **70**, 043515 (2004).
[3] D. J. Schwarz, G. D. Starkman, D. Huterer, and C. J. Copi, Phys. Rev. Lett. **93**, 221301 (2004).
[4] F. K. Hansen, A. J. Banday, and K. M. Gorski, Mon. Not. R. Astron. Soc. **354**, 641 (2004).
[5] A. de Oliveira-Costa, M. Tegmark, M. Zaldarriaga, and A. Hamilton, Phys. Rev. D **69**, 063516 (2004).
[6] K. Land and J. Magueijo, Mon. Not. R. Astron. Soc. **357**, 994 (2005).
[7] K. Land and J. Magueijo, Phys. Rev. Lett. **95**, 071301 (2005).
[8] K. Land and J. Magueijo, Mon. Not. R. Astron. Soc. **362**, 838 (2005).
[9] K. Land and J. Magueijo, Phys. Rev. D **72**, 101302 (2005).
[10] K. Land and J. Magueijo, Mon. Not. R. Astron. Soc. **367**, 1714 (2006).
[11] P. Bielewicz, K. M. Gorski, and A. J. Banday, Mon. Not. R. Astron. Soc. **355**, 1283 (2004).
[12] P. Bielewicz, H. K. Eriksen, A. J. Banday, K. M. Gorski, and P. B. Lilje, Astrophys. J. **635**, 750 (2005).
[13] C. J. Copi, D. Huterer, D. J. Schwarz, and G. D. Starkman, Mon. Not. R. Astron. Soc. **367**, 79 (2006).
[14] C. Copi, D. Huterer, D. Schwarz, and G. Starkman, astro-ph/0605135.
[15] P. D. Naselsky, L. Y. Chiang, P. Olesen, and O. V. Verkhodanov, Astrophys. J. **615**, 45 (2004).
[16] S. Prunet, J. P. Uzan, F. Bernardeau, and T. Brunier, Phys. Rev. D **71**, 083508 (2005).
[17] M. Gluck and C. Pisano, astro-ph/0503442.
[18] A. Stannard and P. Coles, Mon. Not. R. Astron. Soc. **364**, 929 (2005).
[19] A. Bernui, B. Mota, M. J. Reboucas, and R. Tavakol, astro-ph/0511666.
[20] A. Bernui, T. Villela, C. A. Wuensche, R. Leonardi, and I. Ferreira, astro-ph/0601593.
[21] M. Sadegh Movahed, F. Ghasemi, S. Rahvar, and M. Reza Rahimi Tabar, astro-ph/0602461.
[22] P. E. Freeman, C. R. Genovese, C. J. Miller, R. C. Nichol, and L. Wasserman, Astrophys. J. **638**, 1 (2006).
[23] G. Chen and I. Szapudi, Astrophys. J. **635**, 743 (2005).
[24] Y. Wiaux, P. Vielva, E. Martinez-Gonzalez, and P. Vandergheynst, Phys. Rev. Lett. **96**, 151303 (2006).
[25] A. Hajian, T. Souradeep, and N. Cornish, Astrophys. J. **618**, L63 (2005).
[26] A. Hajian and T. Souradeep, astro-ph/0501001.
[27] G. Hinshaw *et al.*, astro-ph/0603451.
[28] This map is available on LAMBDA as part of the three-year data release [27,60–62].
[29] G. F. R. Ellis, Gen. Relativ. Gravit. **2**, 7 (1971).
[30] M. Lachieze-Rey and J. P. Luminet, Phys. Rep. **254**, 135 (1995).
[31] J. Levin, Phys. Rep. **365**, 251 (2002).
[32] A. Linde, J. Cosmol. Astropart. Phys. 10 (2004) 004.
[33] G. F. R. Ellis and M. A. H. MacCallum, Commun. Math. Phys. **12**, 108 (1969).
[34] C. B. Collins and S. W. Hawking, Astrophys. J. **180**, 317 (1973).
[35] C. B. Collins and S. W. Hawking, Mon. Not. R. Astron. Soc. **162**, 307 (1973).
[36] A. G. Doroshkevich, V. N. Lukash, and I. D. Novikov, Sov. Astron. **18**, 554 (1975).
[37] J. D. Barrow, R. Juszkiewicz, and D. H. Sonoda, Mon. Not. R. Astron. Soc. **213**, 917 (1985).
[38] T. R. Jaffe, A. J. Banday, H. K. Eriksen, K. M. Gorski, and F. K. Hansen, Astrophys. J. **643**, 616 (2006).
[39] T. Ghosh, A. Hajian, and T. Souradeep, astro-ph/0604279.
[40] A. Hajian and T. Souradeep, astro-ph/0301590.
[41] A. Hajian, Ph.D. thesis, IUCAA, University of Pune, 2006.
[42] R. Saha, A. Hajian, T. Souradeep, and P. Jain (in preparation).
[43] N. Bartolo, E. Komatsu, S. Matarrese, and A. Riotto, Phys. Rep. **402**, 103 (2004).
[44] E. Komatsu *et al.*, Astrophys. J. Suppl. Ser. **148**, 119 (2003).

[45] D. A. Varshalovich, A. N. Moskalev, and V. K. Khersonskii, *Quantum Theory of Angular Momentum* (World Scientific, Singapore, 1988).
[46] In statistics, an estimator is a function of the known data that is used to estimate an unknown parameter; an estimate is the result from the actual application of the function to a particular set of data. Many different estimators may be possible for any given parameter.
[47] By bias we mean the mismatch between ensemble average of the estimator and the true value.
[48] This is similar to combining a_{lm} to construct the angular power spectrum, $C_l = \frac{1}{2l+1}\sum_m |a_{lm}|^2$, to reduce the cosmic variance.
[49] A. Hajian and T. Souradeep, Astrophys. J. **597**, L5 (2003).
[50] T. Souradeep and A. Hajian, Pramana **62**, 793 (2004).
[51] T. Souradeep and A. Hajian, in *Proceedings of JGRG-14, 2004*, edited by W. Hikida, M. Sasaki, T. Tanaka, and T. Nakamura, Kyoto University, Kyoto.
[52] The WMAP team warns that the original ILC map should not be used for detailed scientific analysis.
[53] http://healpix.jpl.nasa.gov/.
[54] For details of bias correction for BiPS see [26,41].
[55] S. Basak, A. Hajian, and T. Souradeep, Phys. Rev. D **74**, 021301 (2006).
[56] R. Saha, P. Jain, and T. Souradeep, Astrophys. J. **645**, L89 (2006); T. Souradeep, R. Saha, and P. Jain, New Astron. Rev. **50**, 854 (2006).
[57] However it is possible to express any specific individual element of the covariance matrix in terms of linear combinations of BipoSH coefficients to recover such results. We desist from studying these ''unmotivated'' combinations and limit our attention to mathematically well-posed statistics like reduced BiPoSH and BiPS.
[58] T. Souradeep, A. Hajian, and S. Basak, New Astron. Rev. **50**, 889 (2006).
[59] http://lambda.gsfc.nasa.gov/.
[60] N. Jarosik *et al.*, astro-ph/0603452.
[61] L. Page *et al.*, astro-ph/0603450.
[62] D. N. Spergel *et al.*, astro-ph/0603449.